

# Multivariate Sensitivity Analysis of Electric Machine Efficiency Maps and Profiles Under Design Uncertainty

Aylar Partovizadeh\*<sup>✉</sup>, Sebastian Schöps\*<sup>✉</sup>, Dimitrios Loukrezis†<sup>✉</sup>

\*Computational Electromagnetics Group, Technische Universität Darmstadt, 64289 Darmstadt, Germany

†Scientific Computing, Centrum Wiskunde & Informatica (CWI), 1098 XG Amsterdam, The Netherlands

**Abstract**—This work proposes the use of multivariate global sensitivity analysis for assessing the impact of uncertain electric machine design parameters on efficiency maps and profiles. Contrary to the common approach of applying variance-based (Sobol’) sensitivity analysis elementwise, multivariate sensitivity analysis provides a single sensitivity index per parameter, thus allowing for a holistic estimation of parameter importance over the full efficiency map or profile. Its benefits are demonstrated on permanent magnet synchronous machine models of different fidelity. Computations based on Monte Carlo sampling and polynomial chaos expansions are compared in terms of computational cost. The sensitivity analysis results are subsequently used to simplify the models, by fixing non-influential parameters to their nominal values and allowing random variations only for influential parameters. Uncertainty estimates obtained with the full and reduced models confirm the validity of model simplification guided by multivariate sensitivity analysis.

**Index Terms**—driving cycle, efficiency map, electric machine, global sensitivity analysis, Monte Carlo sampling, polynomial chaos expansion, uncertainty quantification.

## I. INTRODUCTION

THE advancement of electric mobility hinges on improving the efficiency of electric machines [1]. This goal concentrates significant research and innovation efforts and places efficiency among the most important quantities of interest (QoIs) in modern electric machine design [2]. Efficiency maps describing the maximum efficiency over the full torque-speed operation range, as well as efficiency profiles corresponding to specific driving cycles, are particularly important tools for assessing the performance of an electric machine for varying and dynamic operating conditions [3], [4].

During the design phase, efficiency maps and profiles are commonly estimated with the help of simulation models, ranging from relatively simple equivalent circuit models (ECMs) to detailed computer-aided design (CAD) models solved with advanced numerical techniques. However, irrespective of resolution capability and approximation accuracy, simulation models are simplified and idealized representations of real-world devices. As such, they do not account for modeling inaccuracies, manufacturing tolerances, material imperfections, or other factors that may arise during the design, fabrication or operation of an electric machine. Taking these uncertainties

into consideration and assessing their impact upon crucial QoIs like efficiency is a significant design challenge.

To that end, uncertainty quantification (UQ) studies are nowadays an important part of model-based electric machine design processes [5]–[18]. One particularly important study is global sensitivity analysis (GSA), which allows to quantitatively attribute the uncertainty observed in a QoI to the uncertain design parameters [19], [20]. GSA results can guide design changes and adjustments, for example, by fixing non-influential parameters and concentrating design efforts on the parameters mainly responsible for QoI variations. Sobol’ GSA is a popular variance-based approach, which quantifies the impact of the uncertain parameters and their combinations upon the QoI’s variability in the form of numerical values known as Sobol’ indices [21]. However, Sobol’ GSA concerns scalar QoIs only, hence, it is not suitable for multivariate QoIs like electric machine efficiency maps and profiles. In such cases, Sobol’ GSA can in principle be applied elementwise, yielding one Sobol’ index per QoI-component. However, this approach runs into problems. First, the number of QoI-components might render this elementwise application computationally demanding, if not prohibitive. Second, it often leads to redundant or difficult to interpret results [22], [23].

While multivariate GSA methods have been introduced [24], [25], their use in engineering design applications remains very limited. For the particular use-case of electric machine design, no relevant studies exist, at least to the knowledge of the authors. This work bridges this gap by demonstrating the application of multivariate GSA to the model-based estimation of efficiency maps and profiles of a permanent magnet synchronous machine (PMSM). In particular, an ECM with uncertain circuit elements and an isogeometric analysis (IGA) model with geometry and material uncertainties are examined. The method allows to identify which uncertain parameters have a significant global impact on the efficiency map or profile and, conversely, which parameters can be safely fixed at nominal values to simplify the model without sacrificing UQ accuracy. To highlight the advantages of multivariate GSA methods, results from the elementwise application of Sobol’ GSA are also presented, showcasing their limitations.

The rest of this paper is organized as follows. In section II we recall the main principles behind the estimation of electric machine efficiency maps and profiles. Section III details variance-based GSA for both scalar and multivariate

Corresponding author: Aylar Partovizadeh (email: aylar.partovizadeh@tu-darmstadt.de).

QoIs, including computation methods based on either Monte Carlo sampling (MCS) [23], [25]–[28] or polynomial chaos expansions (PCEs) [29], [30]. Section IV presents numerical studies based on an ECM and an IGA model of a PMSM. The paper concludes with section V, which summarizes the findings of this work and discusses follow-up research possibilities.

## II. ELECTRIC MACHINE EFFICIENCY MAPS AND PROFILES

Electric machine efficiency, denoted with  $\eta$ , is defined as the ratio of output power  $P_{\text{out}}$  to input power  $P_{\text{in}}$ , such that

$$\eta = \frac{P_{\text{out}}}{P_{\text{in}}} = \frac{P_{\text{out}}}{P_{\text{out}} + P_{\text{loss}}}, \quad (1)$$

where  $P_{\text{loss}}$  represents the total power dissipation due to heat, friction, or other losses [31]. In motoring mode, mechanical power is the useful output, while electrical power is the input. Conversely, in generating mode, electrical power becomes the output, and mechanical power is the input. For PMSMs, the output power is estimated as  $P_{\text{out}} = T \omega_m$ , where  $T$  denotes the torque and  $\omega_m$  the angular velocity. The power loss term is commonly decomposed into three components, such that  $P_{\text{loss}} = P_{\text{elec}} + P_{\text{magn}} + P_{\text{mech}}$ , where  $P_{\text{elec}}$  represents Joule losses in the copper windings of rotor and stator,  $P_{\text{magn}}$  corresponds to hysteresis and eddy current losses in the stator's iron core, and  $P_{\text{mech}}$  accounts for speed-dependent mechanical losses such as friction and windage [32]. The loss components exhibit complex dependencies to the operating points defined by specific  $(T, \omega_m)$  pairs, hence  $P_{\text{loss}} = P_{\text{loss}}(T, \omega_m)$ . Naturally, these dependencies affect efficiency as well.

The efficiency map captures the machine's performance across its operating range by showing the maximum achievable efficiency at each torque-speed combination. Aside from torque and speed values, the maximum efficiency is additionally dependent on operating conditions and constraints, such as current rating, voltage saturation, and thermal limits [33], [34]. In practice, producing an efficiency map entails: (i) discretizing the  $T - \omega_m$  plane into a grid; (ii) computing the maximum efficiency upon that grid; (iii) interpolating the resulting values to create a continuous map. The efficiency map is typically visualized as a contour plot over the torque-speed plane, bounded by an envelope that represents the machine's maximum torque capability across different speed ranges. Efficiency profiles are produced similar to efficiency maps, with the difference that the  $T - \omega_m$  grid is replaced by the operating points defined by the specific driving cycle [4].

## III. VARIANCE-BASED GLOBAL SENSITIVITY ANALYSIS

Sensitivity analysis is broadly defined as “the study of how uncertainty in the output of a model can be apportioned to different sources of uncertainty in the model input” [19]. There exist two main classes of sensitivity analysis methods: local, derivative-based methods that examine variations around a nominal point, and global methods that explore the entire input space [20]. Variance-based methods represent a prominent category within GSA and are the focus of this work. The most well-known variance-based GSA method is the Sobol'

method [21], which however concerns scalar outputs and can only be applied elementwise for multivariate outputs. Multivariate GSA methods were developed later [24], [25]. Sobol' and multivariate GSA, as well as corresponding computation methods, are presented in more detail next.

In the following, we consider a parameter-dependent model  $f(\mathbf{x})$ , such that  $f: \mathbf{x} \rightarrow \mathbf{y}$ , equivalently,  $\mathbf{y} = f(\mathbf{x})$ , where  $\mathbf{x} \in \mathbb{R}^N$  is the input parameter vector and  $\mathbf{y} \in \mathbb{R}^M$  the model output. For  $M = 1$ , the model has a scalar output  $y \in \mathbb{R}$ . The model is assumed to be deterministic, however, the input parameters  $\mathbf{x}$  are assumed to be realizations of a random vector  $\mathbf{X} = (X_1, X_2, \dots, X_N)^\top$ , where  $X_n$ ,  $n = 1, 2, \dots, N$ , are independent random variables. The random vector is defined on the probability space  $(\Theta, \Sigma, P)$ , where  $\Theta$  is the sample space,  $\Sigma$  the sigma algebra of events, and  $P: \Sigma \rightarrow [0, 1]$  a probability measure [35]. For an outcome  $\theta \in \Theta$ ,  $\mathbf{x} = \mathbf{X}(\theta) \in \mathbb{R}^N$  is a random vector realization. The joint probability density function (PDF) of  $\mathbf{X}$  is denoted with  $\varrho_{\mathbf{X}}(\mathbf{x})$ , such that  $\varrho_{\mathbf{X}}: \mathbb{R}^N \rightarrow \mathbb{R}_{\geq 0}$ . Due to the independence assumption,  $\varrho_{\mathbf{X}}(\mathbf{x}) = \prod_{n=1}^N \varrho_{X_n}(x_n)$ , where  $\varrho_{X_n}(x_n)$  are the marginal (univariate) PDFs. Due to the propagation of uncertainty through the model, the output is a random vector dependent on the random input vector, such that  $\mathbf{Y} = f(\mathbf{X})$  [36]. Note that input random fields can also be considered, in which case the Karhunen-Löve expansion (KLE) is typically employed to obtain discrete input random variables  $\mathbf{X} = (X_1, \dots, X_N)$  [36].

### A. Sobol' sensitivity analysis

Assuming a scalar output  $Y = f(\mathbf{X})$  and a square-integrable  $f(\mathbf{X})$ , the output's variance  $\text{Var}(Y)$  can be decomposed as

$$\text{Var}(Y) = \sum_{n=1}^N V_n + \sum_{n < k} V_{nk} + \dots + V_{1, \dots, N}, \quad (2)$$

where  $V_n$  is the variance contribution of  $X_n$  alone,  $V_{nk}$  the contribution of  $X_n$  interacting with  $X_k$ , and so on for higher-order interactions [21]. Then, first-order Sobol' indices are given by

$$S_n = \frac{V_n}{\text{Var}(Y)} = \frac{\text{Var}_{X_n}(\mathbb{E}_{\mathbf{X}_{\sim n}}[Y | X_n])}{\text{Var}(Y)}, \quad (3)$$

where  $\text{Var}_{X_n}(\mathbb{E}_{\mathbf{X}_{\sim n}}[Y | X_n])$  is the first-order effect of  $X_n$  and  $\mathbf{X}_{\sim n}$  denotes the set of all variables except  $X_n$ .  $S_n$  quantifies the fractional contribution of  $X_n$  alone to the output variance. Higher-order indices, for example, second-order indices  $S_{nk} = V_{nk} / \text{Var}(Y)$ , quantify interaction effects. However, computing all  $2^N - 1$  possible indices is often computationally challenging, if not prohibitive. Total-order Sobol' indices provide a more practical alternative by capturing the total effect of  $X_n$  including all interactions. The total effect of  $X_n$  is  $\mathbb{E}_{\mathbf{X}_{\sim n}}[\text{Var}_{X_n}(Y | \mathbf{X}_{\sim n})]$  and the corresponding total-order Sobol' index is given by

$$S_{Tn} = 1 - \frac{V_{\sim n}}{\text{Var}(Y)} = \frac{\mathbb{E}_{\mathbf{X}_{\sim n}}[\text{Var}_{X_n}(Y | \mathbf{X}_{\sim n})]}{\text{Var}(Y)}. \quad (4)$$

The difference  $S_{Tn} - S_n$  quantifies the total interaction effect involving  $X_n$ . That is, if  $S_{Tn} \gg S_n$ , the variable  $X_n$

participates in significant interactions with other parameters. Conversely, if  $S_{Tn} \approx S_n$ ,  $X_n$  has minimal interactions.

### B. Multivariate sensitivity analysis

Assuming a multivariate output  $\mathbf{Y} = f(\mathbf{X})$  with square-integrable  $f(\mathbf{X})$ , the covariance matrix  $\mathbf{C} = \text{Cov}(\mathbf{Y})$  can be decomposed analogously to the (scalar) variance decomposition (2), such that

$$\mathbf{C} = \sum_{n=1}^N \mathbf{C}_n + \sum_{n < k}^N \mathbf{C}_{nk} + \cdots + \mathbf{C}_{1,\dots,N}, \quad (5)$$

where each matrix  $\mathbf{C}_n$ ,  $\mathbf{C}_{nk}$ , etc., represents the covariance contribution from the corresponding subset of input variables [25], [30]. This decomposition captures both main (first-order) effects and interactions across all components of the multivariate output. The trace  $\text{tr}(\mathbf{C})$  corresponds to summing the variances across all output components and is used to obtain scalar sensitivity indices from the covariance decomposition. Then, the first-order generalized sensitivity index for input  $X_n$  is defined as

$$G_n = \frac{\text{tr}(\mathbf{C}_n)}{\text{tr}(\mathbf{C})} = \frac{\sum_{m=1}^M V_n^{(m)}}{\sum_{m=1}^M \text{Var}(Y_m)}, \quad (6)$$

where  $V_n^{(m)}$  quantifies the fractional contribution of  $X_n$  alone to the variance of the  $m$ -th component of the  $M$ -dimensional output. Summing over all output components quantifies the proportion of the total output variance attributable solely to  $X_n$ . Accordingly, the total-order generalized sensitivity index is given by

$$G_{Tn} = 1 - \frac{\text{tr}(\mathbf{C}_{\sim n})}{\text{tr}(\mathbf{C})} = 1 - \frac{\sum_{m=1}^M V_{\sim n}^{(m)}}{\sum_{m=1}^M \text{Var}(Y_m)}, \quad (7)$$

and captures all effects involving  $X_n$ , including its interactions. The difference  $G_{Tn} - G_n$  quantifies the total interaction effect of  $X_n$ . The generalized indices provide a comprehensive assessment of parameter importance for multivariate outputs, while avoiding the interpretability issues associated with the elementwise application of Sobol' GSA [23].

### C. Computation and cost

The two main approaches for computing Sobol' and generalized sensitivity indices are via MCS [23], [25]–[28] or PCE [29], [30]. For either approach, the QoI must be sampled for different realizations of the uncertain model parameters. Denoting the number of samples with  $N_s$ , MCS-based GSA requires additional model sampling on input combinations formed from the original sample. The total sample cost rises to  $N_{\text{GSA}}^{\text{MCS}} = (N+2)N_s$ . It is common for MCS that  $N_s$  is in the order of  $10^3 - 10^5$ , possibly even higher for sufficient convergence. This can result in an undesirable computational cost, especially if the sampled model is computationally expensive.

For PCE-based GSA, the sample is used to compute the PCE coefficients using a least-squares regression [37]. The sensitivity indices are then estimated by simply post-processing the PCE, hence, the cost of PCE-based GSA

is  $N_{\text{GSA}}^{\text{PCE}} = N_s$ . Nonetheless, the computational cost can still become intractable. In particular, for a well-determined regression problem, it is necessary that  $N_s = CK$ , where  $K$  denotes the number of PCE terms and  $C \geq 1$  is an oversampling coefficient [37]. Considering a standard total-degree PCE with maximum polynomial degree  $P$ , the number of PCE terms is equal to  $K = \frac{(N+P)!}{N!P!}$ , which grows rapidly for increasing  $N$ ,  $P$ . The computational burden can be alleviated to some degree with the use of sparse PCEs [38], [39]. Another possible bottleneck is the lack of regularity of  $f(\mathbf{x})$ , which can hinder convergence [40]. Very high dimensional QoIs can also lead to computational issues, which can however in most cases be effectively countered with the use of dimension reduction methods [41]. Nonetheless, PCE can be much more computationally efficient than MCS, especially for smooth models with up to moderately high input dimensions, possibly up to the order of tens if sparse PCEs are employed [38]. MCS should be selected otherwise.

Note that the cost discussion above must be revisited for multivariate outputs like efficiency maps or profiles. In that case, the model must also be sampled on the operating points  $(T, \omega_m)$  that define the map or profile. The number of operating points, denoted with  $N_{\text{op}}$ , becomes an additional factor concerning the sample cost of GSA, which increases to  $N_{\text{GSA}}^{\text{MCS}} = (N+2)N_s N_{\text{op}}$  and  $N_{\text{GSA}}^{\text{PCE}} = N_s N_{\text{op}}$ , respectively.

## IV. APPLICATION TO PERMANENT MAGNET SYNCHRONOUS MACHINE MODELS

As test-case, we consider the benchmark PMSM from the work of Muetze et al. [42]. In Section IV-A, the ECM with four uncertain circuit parameters is examined, first regarding its efficiency map, and second regarding its efficiency profile for the Worldwide Harmonised Light vehicles Test Procedure (WLTP) [43] driving cycle. In Section IV-B, a two-dimensional IGA model with eleven uncertain geometric and material parameters is examined, with respect to its efficiency map in motoring mode only.

### A. Equivalent circuit model

The ECM is depicted in Figure 1. The corresponding semi-analytical computational model is based on the standard voltage and flux-linkage equations in the d-q frame<sup>1</sup> [32]. Efficiency for a given operating point  $(T, \omega_m)$  can be estimated in a few milliseconds. The four circuit elements, listed in Table I, are treated as uncertain and assumed to vary uniformly within  $\pm 5\%$  of their nominal values.

1) *Sensitivity analysis of efficiency map*: The efficiency map is evaluated on a grid of  $N_{\text{op}} = 232$  operating points  $(T, \omega_m)$ , uniformly distributed over the operating range. Figures 2a and 2b display the mean and standard deviation of the efficiency map, computed with MCS and a sample of  $N_s^{\text{MCS}} = 2 \cdot 10^5$  model evaluations. Nearly identical results are obtained with a total-degree PCE with maximum polynomial degree  $P = 2$  and oversampling coefficient  $C = 2$ ,

<sup>1</sup>The computational model will be made available at a dedicated Zenodo repository upon acceptance of the paper.

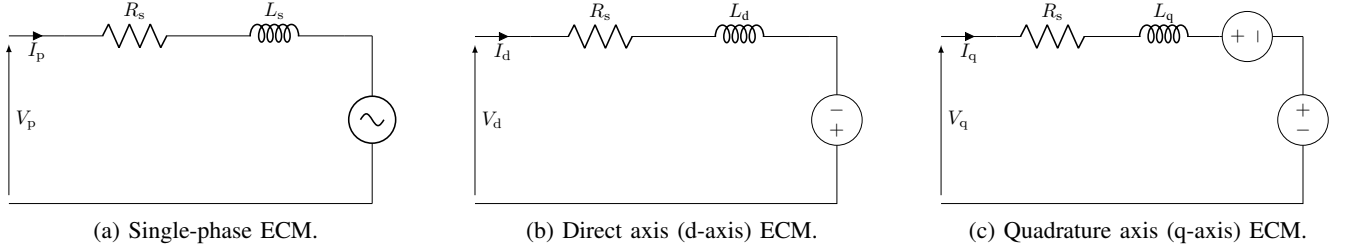


Fig. 1: PMSM ECM.

TABLE I  
PARAMETERS OF THE PMSM ECM.

Parameter	Symbol	Nominal value	Units
Phase resistance	$R_s$	8.9462	$\Omega$
Magnet flux linkage	$\lambda$	0.1144	Wb
d-axis inductance	$L_d$	0.2055	H
q-axis inductance	$L_q$	0.332	H

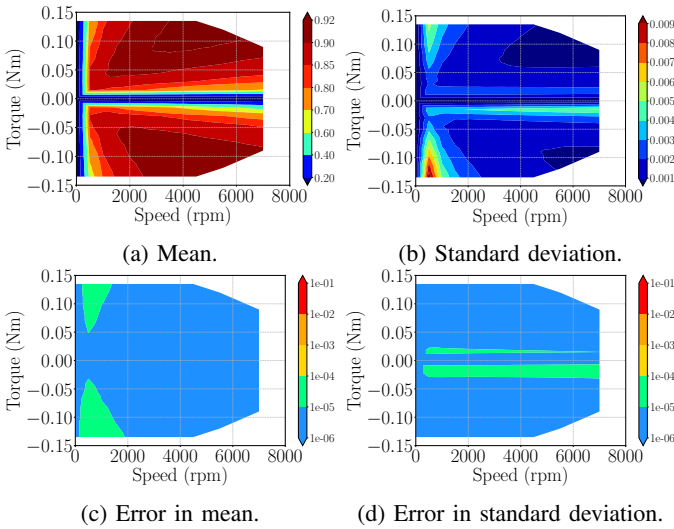


Fig. 2: Mean and standard deviation of the ECM's efficiency map, along with pointwise absolute errors between MCS- and PCE-based estimates.

which corresponds to a sample size  $N_s^{\text{PCE}} = 30$ . Figures 2c and 2d show the pointwise errors for mean and standard deviation, respectively. Similar errors are obtained for the GSA results, therefore, only one set of results is presented in the following. For the aforementioned sample sizes, the MCS-based GSA requires  $N_{\text{GSA}}^{\text{MCS}} = N_s^{\text{MCS}} (5 + 2) N_{\text{op}} = 3.25 \cdot 10^8$  model evaluations. The PCE-based approach needs  $N_{\text{GSA}}^{\text{PCE}} = N_s^{\text{PCE}} N_{\text{op}} = 6.96 \cdot 10^3$ , further highlighting its advantage in terms of computational efficiency.

Figure 3 illustrates the results of Sobol' GSA applied elementwise, which yields one sensitivity map per uncertain parameter. Only first-order Sobol' indices are displayed; total-order indices are almost identical, suggesting negligible parameter interactions. The Sobol' GSA results reveal that  $R_s$  and  $\lambda$  have a significant influence on efficiency. In contrast, the contribution of  $L_d$  is negligible across the entire grid, while  $L_q$  appears to have some localized importance for certain

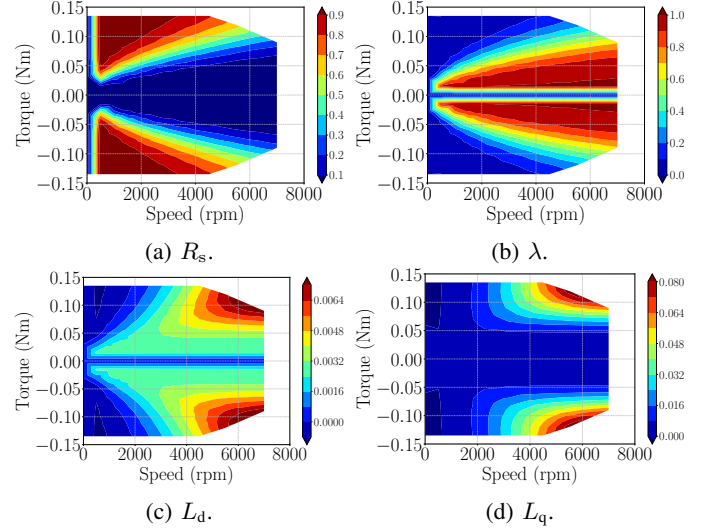


Fig. 3: Elementwise Sobol' GSA of the ECM's efficiency map. Only first-order indices are shown, due to negligible higher order interactions.

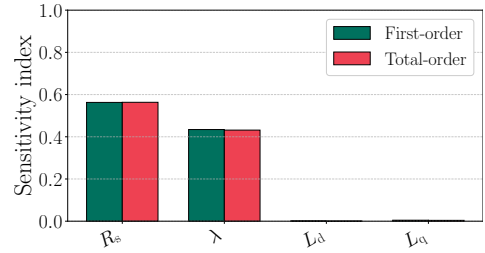


Fig. 4: Multivariate GSA of the ECM's efficiency map.

operating conditions. These results should be interpreted in the context of the efficiency map's standard deviation, shown in Figure 2b. The standard deviation is close to zero in the high-torque and high-speed regions of the map, where the Sobol' indices of  $L_q$  have comparatively large values. Therefore, the Sobol' index values of  $L_q$  in these regions are likely numerical artifacts and do not convey useful sensitivity information.

Figure 4 presents the multivariate GSA results. The first- and total-order generalized sensitivity indices are nearly identical, further indicating negligible parameter interactions. Multivariate GSA reinforces the earlier findings regarding relative parameter importance. Furthermore, these results suggest that the high Sobol' index values observed for  $L_q$  in Figure 3 are indeed misleading.

TABLE II  
MAES IN EFFICIENCY MAP MEAN AND STANDARD  
DEVIATION ESTIMATES BETWEEN THE FULL AND REDUCED  
ECM.

Fixed parameters	MAE, mean	MAE, st.d.
$L_d, L_q$	$1.08 \cdot 10^{-5}$	$8.77 \cdot 10^{-6}$

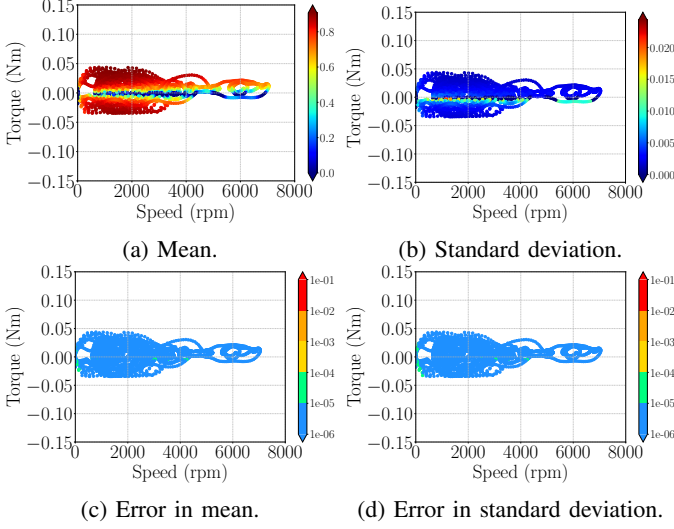


Fig. 5: Mean and standard deviation of the ECM's efficiency profile, along with pointwise absolute errors between MCS- and PCE-based estimates.

To validate the GSA results, mean absolute errors (MAEs) in the mean and standard deviation estimates obtained with the full ECM, i.e., with random variations in all four parameters, and with a reduced ECM with fixed  $L_q$  and  $L_d$ , are computed and presented in Table II. The errors in both mean and standard deviation are very low, supporting the previous observations.

2) *Sensitivity analysis of efficiency profile*: The WLTP driving cycle is defined by  $N_{op} = 3601$  operating points  $(T, \omega_m)$ , which is one magnitude higher than the efficiency map grid used in Section IV-A1. Due to the large number of operating points, MCS-based GSA becomes too computationally demanding, even for the computationally inexpensive ECM evaluations. Therefore, only PCE-based GSA results are reported in this section.

The mean and standard deviation of the efficiency profile are displayed in Figures 5a and 5b. These results are obtained using MCS with sample size  $N_s^{MC} = 2 \cdot 10^5$ . Almost identical results are obtained using a total-degree PCEs with maximum polynomial degree  $P = 4$  and oversampling coefficient  $C = 5$ , which corresponds to a sample size  $N_s^{PCE} = 350$ . The pointwise errors in mean and standard deviation are respectively shown in Figures 5c and 5d. The same PCE is used for the GSA results reported in the following.

Figure 6 presents the elementwise Sobol' GSA results for the efficiency profile. Figure 7 shows the corresponding multivariate GSA results. Both Sobol' and multivariate GSA consistently identify  $L_d$  and  $L_q$  as non-influential. However, while in section IV-A1  $\lambda$  exhibited slightly smaller relative

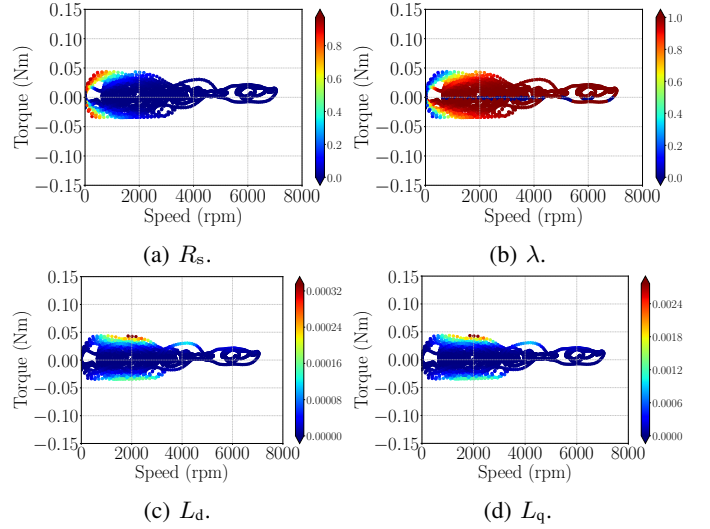


Fig. 6: Elementwise Sobol' GSA of the ECM's efficiency profile. Only first-order indices are shown, due to negligible higher order interactions.

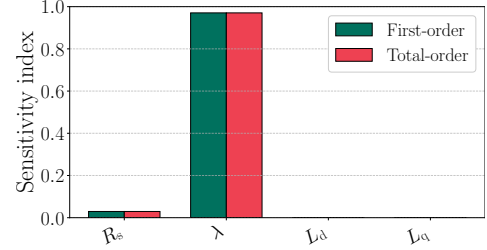


Fig. 7: Multivariate GSA of the ECM's efficiency profile.

TABLE III  
MAES IN EFFICIENCY PROFILE MEAN AND STANDARD  
DEVIATION ESTIMATES BETWEEN THE FULL AND REDUCED  
ECM.

Fixed parameters	MAE, mean	MAE, st.d.
$L_d, L_q$	$3.0 \cdot 10^{-6}$	$4.0 \cdot 10^{-6}$

importance than  $R_s$ , here it is the dominant parameter. This difference can be attributed to the fact that the driving cycle does not fully cover the entire operating range. In particular, the high-torque regions where  $R_s$  had high sensitivity indices (see Figure 3), are not represented in the driving cycle.

Table III reports MAEs in the mean and standard deviation of the efficiency profile between full and reduced PMSM ECMs. The results confirm that parameters deemed as non-influential by multivariate GSA can be fixed to their nominal values without significantly affecting UQ accuracy.

### B. Isogeometric analysis model

The IGA model of the PMSM is implemented in MATLAB using the `GeoPDES` package [44]. The model is based on standard finite element modeling [45], where the basis functions coincide with the CAD spline basis [46]. Eleven model parameters are considered to be uncertain, each assumed

TABLE IV  
PARAMETERS OF THE PMSM IGA MODEL.

Parameter	Symbol	Nominal Value	Units
Stator outer radius	SRO	0.0565	m
Yoke height	HY	0.00116	m
Slot opening height	HSO	0.00098	m
Tooth width	WT	0.00148	m
Slot opening width	WSO	0.00323	m
Magnet height	HM	0.00435	m
Rotor inner radius	RRI	0.008	m
Magnet circumference ratio	MR	0.5	-
$BH$ -curve scaling factor	SF	1.0	-
Phase resistance	$R_s$	4.475	$\Omega$
Magnet remanence	$B_r$	0.41	T

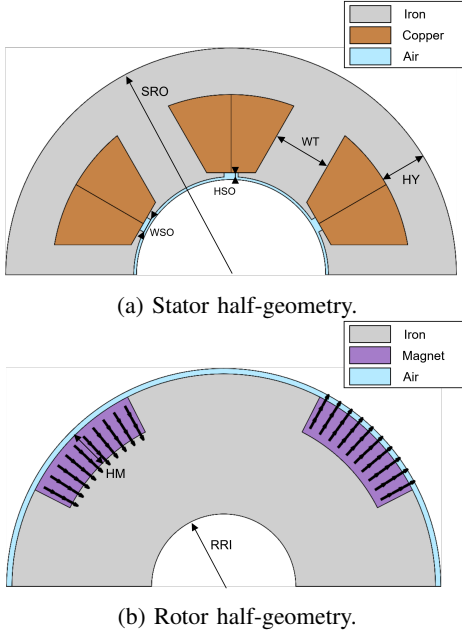


Fig. 8: PMSM half-geometry in two dimensions.

to vary uniformly within  $\pm 5\%$  of its nominal value. The parameters and their nominal values are listed in Table IV. The geometry of the PMSM is illustrated in Figure 8, along with the uncertain geometric parameters, with the exception of the magnet circumference ratio (MR).

Compared to the ECM used previously, the IGA model introduces a number of challenges. First, due to its much higher computational cost, MCS is rendered unusable, both for statistics estimates and for GSA. Second, it becomes too computationally expensive to evaluate the model over its full operating range, as well as for the WLTP driving cycle. Last, the comparatively high input dimensionality ( $N = 11$ ) results in large numbers of total-degree PCE terms, even for moderate polynomial degrees  $P$ . In turn, generating a sufficiently large sample amounts to an undesirable computational cost. To render the computational cost tractable, the PMSM is operated solely in motoring mode and GSA is confined to efficiency maps only. Using a grid of  $N_{op} = 116$  operating points ( $T, \omega_m$ ), a single efficiency map is computed in approximately 800 seconds. Additionally, the use of PCE is enabled by adaptive basis construction algorithms [47], [48]. Samples

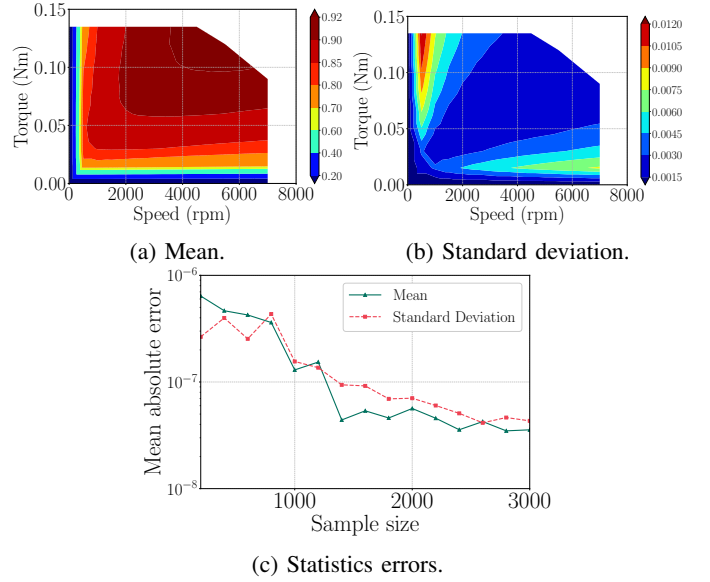


Fig. 9: Mean and standard deviation of the IGA model's efficiency map, with MAEs for increasing sample sizes. The MAEs are computed with respect to reference values obtained with a PCE trained on the dataset of maximum size  $N_{s,max} = 3300$ .

TABLE V  
MAES IN EFFICIENCY MAP MEAN AND STANDARD DEVIATION ESTIMATES BETWEEN THE FULL AND REDUCED IGA MODEL.

Fixed parameters	MAE, mean	MAE, st.d.
SF, HSO, WSO, HM, RRI	$5.77 \cdot 10^{-6}$	$3.45 \cdot 10^{-6}$

of increasing sizes are employed, up to a maximum size  $N_s^{max} = 3300$ .

Figures 9a and 9b display the mean and standard deviation of the efficiency map estimated with the adaptive PCE trained on the largest available sample. Figure 9c shows the corresponding MAEs for samples on increasing size. As can be observed, the MAEs are below  $10^{-6}$  already for very small sample sizes. Figure 10 presents the results of the elementwise Sobol' GSA, while Figure 11 displays the multivariate GSA results. In both cases, only first-order indices are shown; total-order indices are nearly identical, indicating negligible parameter interactions. The two GSA methods are in agreement that MR, SRO, HY, WT,  $B_r$ , and  $R_s$  have a significant influence on efficiency variation. Conversely, SF, HSO, WSO, HM, and RRI exhibit negligible influence. The results of GSA are verified by comparing mean and standard deviation estimates based on the full IGA model with all eleven uncertain parameters, and with a reduced model where the five non-influential parameters are fixed to their nominal values. The low MAE values between the two models, shown in Table V, confirm the GSA results.

## V. SUMMARY AND CONCLUSIONS

This work demonstrated the use of multivariate GSA for assessing the impact of uncertain electric machine design

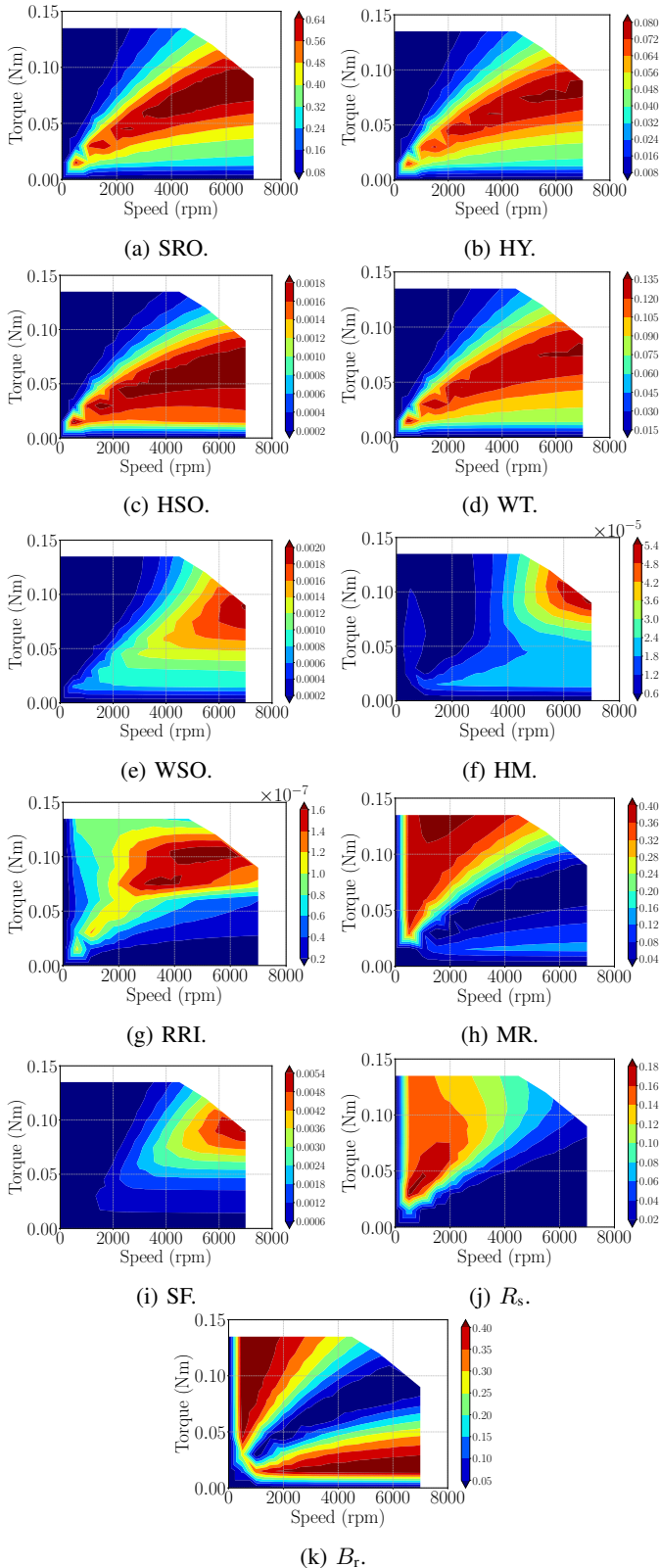


Fig. 10: Elementwise Sobol' GSA of the IGA model's efficiency map. Only first-order indices are shown, due to negligible higher-order interactions.

parameters on efficiency maps and profiles. Using two models of a PMSM, namely, an ECM and an IGA model, we showcase

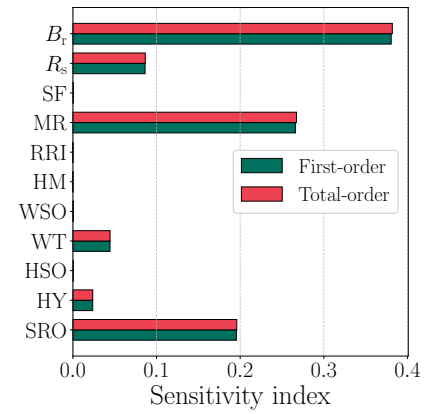


Fig. 11: Multivariate GSA of the IGA model's efficiency map.

the shortcomings of the Sobol' GSA method applied elementwise, as well as the benefits of multivariate GSA. The latter overcomes the limitations of Sobol GSA with the use of generalized sensitivity indices tailored to multidimensional QoIs. In addition, we compare GSA based on MCS and PCE, and find that the latter is be much more computationally efficient for the selected test-cases. Last, we leverage the results of GSA for model simplification, by fixing the parameters identified as non-influential to their nominal values. In the numerical test-cases of this work, 45% to 60% of the initially considered uncertain parameters can be fixed without compromising the accuracy of UQ results.

We conclude that multivariate GSA should be the preferred tool for assessing the sensitivity of efficiency maps and profiles to uncertain electric machine design parameters. Follow-up works will investigate the applicability of multivariate GSA to other multidimensional QoIs, e.g., torque signals or field distributions. More challenging test-cases will also be investigated, e.g., ones involving higher-dimensional inputs and QoIs.

#### ACKNOWLEDGMENTS

The authors are partially supported by the joint DFG/FWF Collaborative Research Centre CREATOR (DFG: Project-ID 492661287/TRR 361; FWF: 10.55776/F90) at TU Darmstadt, TU Graz, and JKU Linz. The authors thank P. K. Dhakal, K. Heidarikani, and A. Muetze for providing the PMSM ECM, and M. Wiesheu for providing the IGA model.

#### REFERENCES

- [1] K. Heineke, P. Kampshoff, and T. Möller, "Spotlight on mobility trends," *McKinsey & Company*, 2024.
- [2] M. Gobbi, A. Sattar, R. Palazzetti, and G. Mastinu, "Traction motors for electric vehicles: Maximization of mechanical efficiency—a review," *Applied Energy*, vol. 357, p. 122496, 2024.
- [3] E. Roshandel, A. Mahmoudi, S. Kahourzade, and W. L. Soong, "Efficiency maps of electrical machines: A tutorial review," *IEEE Transactions on Industry Applications*, vol. 59, no. 2, pp. 1263–1272, 2022.
- [4] P. K. Dhakal, K. Heidarikani, R. Seebacher, and A. Muetze, "A comparative study on drive cycle performance of laboratory PMSMs using efficiency maps and time-stepping approaches," *Energies*, vol. 18, no. 21, p. 5802, 2025.
- [5] R. Ramarotafika, A. Benabou, and S. Clenet, "Stochastic modeling of soft magnetic properties of electrical steels: Application to stators of electrical machines," *IEEE Transactions on Magnetics*, vol. 48, no. 10, pp. 2573–2584, 2012.

- [6] M. Fratila, R. Ramarotafika, A. Benabou, S. Clénet, and A. Tounzi, "Stochastic post-processing calculation of iron losses—application to a PMSM," *COMPEL - The international journal for computation and mathematics in electrical and electronic engineering*, vol. 32, no. 4, pp. 1383–1392, 2013.
- [7] S. Clénet, "Uncertainty quantification in computational electromagnetics: The stochastic approach," *International Compumag Society Newsletters*, vol. 20, no. 1, pp. 2–12, 2013.
- [8] P. Offermann, H. Mac, T. T. Nguyen, S. Clénet, H. De Gersem, and K. Hameyer, "Uncertainty quantification and sensitivity analysis in electrical machines with stochastically varying machine parameters," *IEEE Transactions on Magnetics*, vol. 51, no. 3, pp. 1–4, 2015.
- [9] Z. Bontinck, H. De Gersem, and S. Schöps, "Response surface models for the uncertainty quantification of eccentric permanent magnet synchronous machines," *IEEE Transactions on Magnetics*, vol. 52, no. 3, pp. 1–4, 2015.
- [10] A. Belahcen, P. Rasilo, T.-T. Nguyen, and S. Clénet, "Uncertainty propagation of iron loss from characterization measurements to computation of electrical machines," *COMPEL - The international journal for computation and mathematics in electrical and electronic engineering*, vol. 34, no. 3, pp. 624–636, 2015.
- [11] S. Liu, H. Mac, S. Clénet, T. Coorevits, and J.-C. Mipo, "Study of the influence of the fabrication process imperfections on the performance of a claw pole synchronous machine using a stochastic approach," *IEEE Transactions on Magnetics*, vol. 52, no. 3, pp. 1–4, 2015.
- [12] A. Galetzka, Z. Bontinck, U. Römer, and S. Schöps, "A multilevel Monte Carlo method for high-dimensional uncertainty quantification of low-frequency electromagnetic devices," *IEEE Transactions on Magnetics*, vol. 55, no. 8, pp. 1–12, 2019.
- [13] A. Beltran-Pulido, D. Aliprantis, I. Bilonis, A. R. Munoz, F. Leonardi, and S. M. Avery, "Uncertainty quantification and sensitivity analysis in a nonlinear finite-element model of a permanent magnet synchronous machine," *IEEE Transactions on Energy Conversion*, vol. 35, no. 4, pp. 2152–2161, 2020.
- [14] G. Lei, G. Bramerdorfer, B. Ma, Y. Guo, and J. Zhu, "Robust design optimization of electrical machines: Multi-objective approach," *IEEE Transactions on Energy Conversion*, vol. 36, no. 1, pp. 390–401, 2020.
- [15] Y. Yang, C. Zhang, G. Bramerdorfer, N. Bianchi, J. Qu, J. Zhao, and S. Zhang, "A computationally efficient surrogate model based robust optimization for permanent magnet synchronous machines," *IEEE Transactions on Energy Conversion*, vol. 37, no. 3, pp. 1520–1532, 2022.
- [16] H. Liu, X. Jin, N. Bianchi, G. Bramerdorfer, P. Hu, C. Zhang, and Y. Yang, "A permanent magnet assembling approach to mitigate the cogging torque for permanent magnet machines considering manufacturing uncertainties," *Energies*, vol. 15, no. 6, p. 2154, 2022.
- [17] D. Liang, Z.-Q. Zhu, P. Taras, R. Nilifard, Z. Azar, and N. Madani, "Sensitivity analysis and uncertainty quantification of thermal behavior for permanent magnet synchronous machines," *IEEE Access*, vol. 12, pp. 65 386–65 402, 2024.
- [18] A. Partovizadeh, S. Schöps, and D. Loukrezis, "Fourier-enhanced reduced-order surrogate modeling for uncertainty quantification in electric machine design," *Engineering with Computers*, vol. 41, pp. 2619–2639, 2025.
- [19] A. Saltelli, S. Tarantola, F. Campolongo, and M. Ratto, *Sensitivity analysis in practice: a guide to assessing scientific models*. Wiley Online Library, 2004, vol. 1.
- [20] A. Saltelli, M. Ratto, T. Andres, F. Campolongo, J. Cariboni, D. Gatelli, M. Saisana, and S. Tarantola, *Global sensitivity analysis: the primer*. John Wiley & Sons, 2008.
- [21] I. Sobol', "Global sensitivity indices for nonlinear mathematical models and their Monte Carlo estimates," *Mathematics and Computers in Simulation*, vol. 55, no. 1, pp. 271–280, 2001.
- [22] M. Lamboni, D. Makowski, S. Lehuger, B. Gabrielle, and H. Monod, "Multivariate global sensitivity analysis for dynamic crop models," *Field Crops Research*, vol. 113, no. 3, pp. 312–320, 2009.
- [23] M. Lamboni, H. Monod, and D. Makowski, "Multivariate sensitivity analysis to measure global contribution of input factors in dynamic models," *Reliability Engineering & System Safety*, vol. 96, no. 4, pp. 450–459, 2011.
- [24] K. Campbell, M. D. McKay, and B. J. Williams, "Sensitivity analysis when model outputs are functions," *Reliability Engineering & System Safety*, vol. 91, no. 10–11, pp. 1468–1472, 2006.
- [25] F. Gamboa, A. Janon, T. Klein, and A. Lagnoux, "Sensitivity indices for multivariate outputs," *Comptes Rendus. Mathématique*, vol. 351, no. 7–8, pp. 307–310, 2013.
- [26] M. J. Jansen, "Analysis of variance designs for model output," *Computer Physics Communications*, vol. 117, no. 1–2, pp. 35–43, 1999.
- [27] A. Saltelli, P. Annoni, I. Azzini, F. Campolongo, M. Ratto, and S. Tarantola, "Variance based sensitivity analysis of model output. design and estimator for the total sensitivity index," *Computer Physics Communications*, vol. 181, no. 2, pp. 259–270, 2010.
- [28] F. Gamboa, A. Janon, T. Klein, A. Lagnoux, and C. Prieur, "Statistical inference for Sobol pick-freeze Monte Carlo method," *Statistics*, vol. 50, no. 4, pp. 881–902, 2016.
- [29] B. Sudret, "Global sensitivity analysis using polynomial chaos expansions," *Reliability Engineering & System Safety*, vol. 93, no. 7, pp. 964–979, 2008.
- [30] O. Garcia-Cabrejo and A. Valocchi, "Global sensitivity analysis for multivariate output using polynomial chaos expansion," *Reliability Engineering & System Safety*, vol. 126, pp. 25–36, 2014.
- [31] E. Roshandel, A. Mahmoudi, S. Kahourzade, A. Yazdani, and G. Shafiqullah, "Losses in efficiency maps of electric vehicles: An overview," *Energies*, vol. 14, no. 22, p. 7805, 2021.
- [32] R. Krishnan, *Permanent magnet synchronous and brushless DC motor drives*. CRC press, 2017.
- [33] S. Kahourzade, A. Mahmoudi, W. L. Soong, N. Ertugrul, and G. Pellegrino, "Estimation of PM machine efficiency maps from limited data," *IEEE Transactions on Industry Applications*, vol. 56, no. 3, pp. 2612–2621, 2020.
- [34] S.-W. Hwang, J.-Y. Ryu, J.-W. Chin, S.-H. Park, D.-K. Kim, and M.-S. Lim, "Coupled electromagnetic-thermal analysis for predicting traction motor characteristics according to electric vehicle driving cycle," *IEEE Transactions on Vehicular Technology*, vol. 70, no. 5, pp. 4262–4272, 2021.
- [35] R. C. Smith, *Uncertainty quantification: theory, implementation, and applications*. SIAM, 2024.
- [36] W. Betz, I. Papaioannou, and D. Straub, "Numerical methods for the discretization of random fields by means of the Karhunen–Loève expansion," *Computer Methods in Applied Mechanics and Engineering*, vol. 271, pp. 109–129, 2014.
- [37] G. Migliorati, F. Nobile, E. Von Schwerin, and R. Tempone, "Analysis of discrete  $L^2$  projection on polynomial spaces with random evaluations," *Foundations of Computational Mathematics*, vol. 14, no. 3, pp. 419–456, 2014.
- [38] N. Lüthen, S. Marelli, and B. Sudret, "Sparse polynomial chaos expansions: Literature survey and benchmark," *SIAM/ASA Journal on Uncertainty Quantification*, vol. 9, no. 2, pp. 593–649, 2021.
- [39] —, "Automatic selection of basis-adaptive sparse polynomial chaos expansions for engineering applications," *International Journal for Uncertainty Quantification*, vol. 12, no. 3, 2022.
- [40] A. Galetzka, D. Loukrezis, N. Georg, H. De Gersem, and U. Römer, "An hp-adaptive multi-element stochastic collocation method for surrogate modeling with information re-use," *International Journal for Numerical Methods in Engineering*, vol. 124, no. 12, pp. 2902–2930, 2023.
- [41] C. K. J. Hou and K. Behdinan, "Dimensionality reduction in surrogate modeling: A review of combined methods," *Data Science and Engineering*, vol. 7, no. 4, pp. 402–427, 2022.
- [42] A. Muetze, K. Heidarikani, P. K. Dhakal, R. Seebacher, and S. Schöps, "'CREATOR case': PMSM and IM electric machine data for validation and benchmarking of simulation and modeling approaches," *COMPEL - The international journal for computation and mathematics in electrical and electronic engineering*, 2025.
- [43] P. Mock, J. Kühlwein, U. Tietge, V. Franco, A. Bandivadekar, and J. German, "The WLTP: How a new test procedure for cars will affect fuel consumption values in the EU," *International Council on Clean Transportation*, vol. 9, no. 3547, pp. 1–20, 2014.
- [44] R. Vázquez, "A new design for the implementation of isogeometric analysis in Octave and Matlab: GeoPDEs 3.0," *Computers & Mathematics with Applications*, vol. 72, no. 3, pp. 523–554, 2016.
- [45] S. J. Salon, *Finite element analysis of electrical machines*. Kluwer academic publishers Boston, 1995, vol. 101.
- [46] M. Wiesheu, T. Komann, M. Merkel, S. Schöps, S. Ulbrich, and I. Cortes Garcia, "Combined parameter and shape optimization of electric machines with isogeometric analysis," *Optimization and Engineering*, vol. 26, no. 2, pp. 1011–1038, 2025.
- [47] D. Loukrezis, A. Galetzka, and H. De Gersem, "Robust adaptive least squares polynomial chaos expansions in high-frequency applications," *International Journal of Numerical Modelling: Electronic Networks, Devices and Fields*, vol. 33, no. 6, p. e2725, 2020.
- [48] D. Loukrezis, E. Diehl, and H. De Gersem, "Multivariate sensitivity-adaptive polynomial chaos expansion for high-dimensional surrogate modeling and uncertainty quantification," *Applied Mathematical Modelling*, vol. 137, p. 115746, 2025.